Journal of Alloys and Compounds 509 (2011) 9060–9064

Contents lists available at ScienceDirect

Journal of Alloys and Compounds

journal homepage: www.elsevier.com/locate/jallcom

Microstructure and mechanical properties of SiC-nanowire-augmented tungsten composites

Dongju Lee [a], Heesub Park [a], Hojin Ryu [b], Seokwoo Jeon [a], Soonhyung Hong [a,*]

[a] Department of Materials Science and Engineering, Korea Advanced Institute of Science and Technology, 335 Science Road, Yuseong-gu, Daejeon 305-701, Republic of Korea
[b] DUPIC, Korea Atomic Energy Research Institute, 150 Deokjin-dong, Yuseong-gu, Daejeon 305-353, Republic of Korea

ARTICLE INFO

Article history:
Received 14 March 2011
Received in revised form 31 May 2011
Accepted 1 June 2011
Available online 25 June 2011

Keywords:
Metal matrix composites
Powder metallurgy
Sintering
Microstructure
Mechanical properties

ABSTRACT

The effect of an addition of SiC nanowire on the microstructure and mechanical properties of tungsten-based composites is investigated in this study. SiC-nanowire-augmented tungsten composites were prepared by a spray-drying process and an in situ spark plasma sintering process. Three distinctive reaction phases, tungsten, tungsten carbide (W_2C) and rod-type tungsten silicide (W_5Si_3) were formed during the sintering process. The flexural strength was significantly increased from 706 MPa to 924 MPa in tungsten composites augmented with SiC nanowires, as was the formation of W_2C and W_5Si_3 phases. The rod-type W_5Si_3 bears significant stress by both sharing a portion of the load and providing a bridging mechanism. Furthermore, a high ablation resistance at an elevated temperature was observed for tungsten composites augmented with SiC nanowires.

1. Introduction

Recently, tungsten-based composites have gained considerable attention owing to their excellent performance levels at high temperatures due to exceptional high temperature properties such as a high melting point (3410 °C), a high modulus (310–380 GPa), good thermal conductivity (105 ± 10 W/m K), and a low thermal expansion coefficient (4.5×10^{-6}/K) [1,2]. Therefore tungsten-based composites are promising candidates for aerospace applications such as heat shields, combustion chamber liners and rock nozzles, or structural material for fusion reactors [3,4]. However, tungsten is associated with a serious reduction in its strength at elevated temperatures [5]. It is well known that this deterioration in strength is due to the oxidation of the surface of tungsten at high temperatures, thus requiring that its microstructure be controlled to secure feasible performance at high temperatures [6]. Hence, many studies have been undertaken to reduce the oxidation of tungsten and to control its microstructure through surface coatings and with the application of additives such as SiC, HfC, ZrC, or La_2O_3 to the tungsten matrix [7–10]. Through such studies, SiC has become well known as an additive and a coating material for tungsten-based composites due to the excellent thermal shock resistance, strength, toughness and oxidation resistance it offers [11]. Baud et al. [12] showed that W_2C and W_5Si_3 phases form in a reaction between W and SiC at temperatures that exceed 1473 K. Although the chemical reactions of SiC/W composites have been thoroughly investigated, information about the microstructures and mechanical properties of SiC/W composites are limited [13]. Therefore, in this study, the shape of W_5Si_3 is controlled via the initial SiC shape through mixing with W powder to improve the strength of SiC-augmented tungsten composites. In addition, the effects of the microstructures and the volume fraction on the flexural strength of SiC-augmented tungsten composites are investigated. The mass ablation rate of SiC-augmented tungsten composites is also identified.

2. Experimental

To fabricate SiC-augmented tungsten composite (SiC_{NW}/W) powders, ammonium meta tungstate (AMT, $(NH_4)_6H_2W_{12}O_{40}\cdot xH_2O$, as a tungsten precursor) and SiC nanowires were used. The SiC nanowires were synthesized by the reaction between carbon nanotubes (CNTs) (Hanwha Nanotech, at a diameter of 10–15 nm and a length of 10–20 μm) and SiO powder (Sigma–Aldrich, 325 mesh) [14,15]. The reaction was carried out in a vacuum furnace at 1350 °C under a pressure of 100 mTorr for 30 min. The SiC nanowires were sonicated for 2 h in distilled water to obtain a homogeneous dispersion. AMT was added to a suspension with SiC nanowires and these were then sonicated for 2 h. This solution was spray dried to fabricate homogeneously mixed SiC nanowire/W composite powders at an atomizing pressure of 120 kPa, a spray drying temperature of 200 °C, blowing at 0.13 m^3/min and at a feed rate of 400 ml/h. The dried composite powders were then calcined at 500 °C for 1 h in air. The calcined SiC nanowire/WO_3 composite powders were reduced at 800 °C for 2 h under a hydrogen atmosphere. The volume fractions of SiC nanowire varied from 0 vol.% to 20 vol.%.

The SiC_{NW}/W powders were consolidated by a spark plasma sintering process (SPS) [16]. The composite powders were compacted in a graphite mold and heated by a pulsed electric current, after which they were sintered at 1700 °C for 3 min

* Corresponding author. Tel.: +82 42 350 3327; fax: +82 42 350 3310.
E-mail address: shhong@kaist.ac.kr (S. Hong).

0925-8388/$ – see front matter © 2011 Elsevier B.V. All rights reserved.
doi:10.1016/j.jallcom.2011.06.005

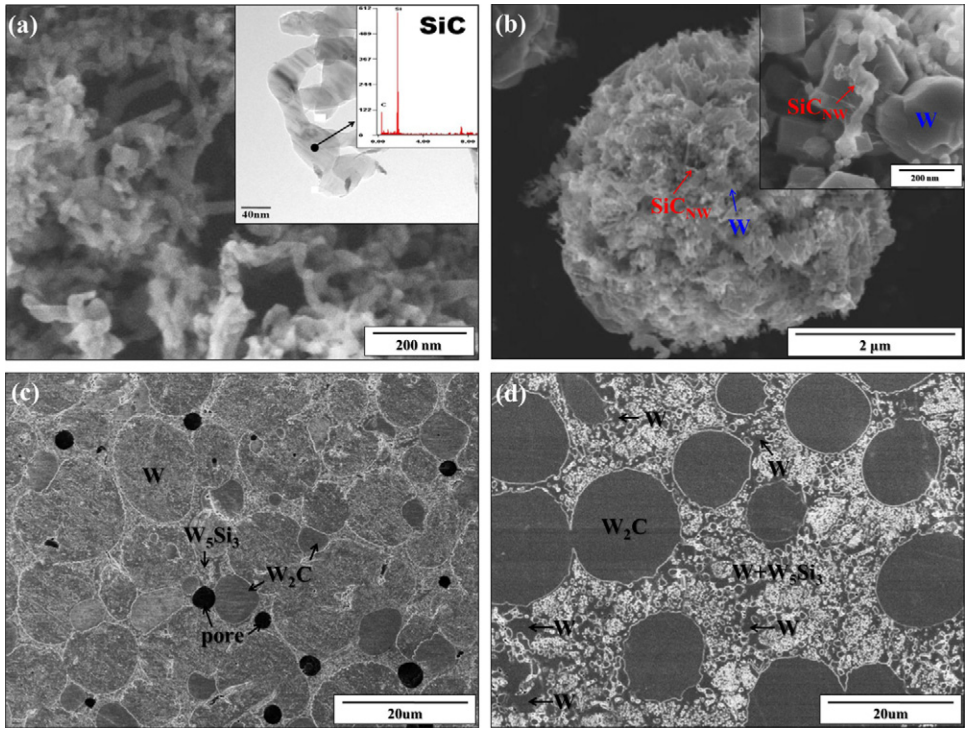

Fig. 1. (a) Microstructure of SiC nanowires synthesized by a reaction between CNT and SiO. (b) SEM micrographs of 20 vol.% SiC_{NW}/W composite powder in which SiC nanowires were homogeneously mixed with W powder. SEM micrographs showing 5 vol.% SiC_{NW}/W composites (c) and 20 vol.% SiC_{NW}/W composites, (d) as revealed after chemical etching.

under an applied pressure of 50 MPa under vacuum pressure. The heating rate was maintained at 100 °C/min up to the sintering temperature. The microstructures of the sintered composites were examined using high-resolution scanning electron microscopy (SEM, Hitachi S-4800), and the volume fractions of W, W_2C and W_5Si_3 in the SiC_{NW}/W composites were determined using an image analysis program (Matrox Inspector 2), as well as through X-ray diffraction (XRD) patterns (RigakuD/MAX-IIIC) and transmission electron microscopy (TEM, Tecnai F30). The tungsten, tungsten carbide and tungsten silicide phases were identified using the diffraction pattern database maintained by the Joint Committee for Powder Diffraction Studies (JCPDS). The flexural strength of the SiC_{NW}/W composites was measured using an INSTRON

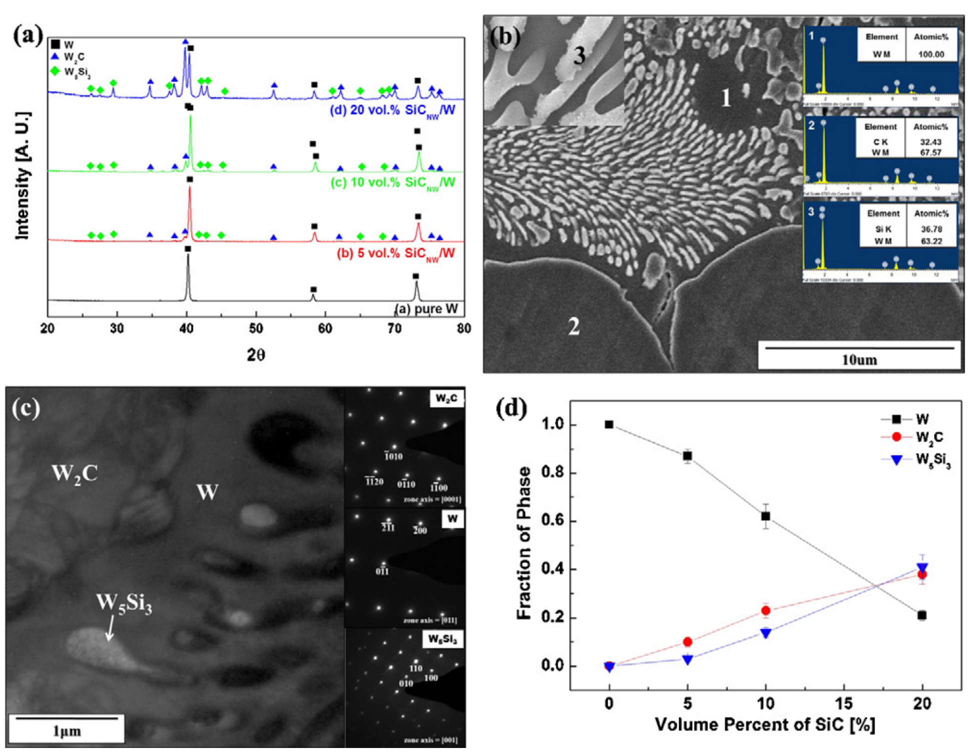

Fig. 2. (a) XRD patterns of sintered the SiC_{NW}/W composite at 1700 °C for 3 min. (b) Elemental analysis of the different regions of the 20 vol.% SiC_{NW}/W composites with EDS. (c) TEM micrograph and selected-area electron diffraction patterns of each phase in 20 vol.% SiC_{NW}/W composites. (d) Volume fraction of each phase while varying the SiC volume fraction.

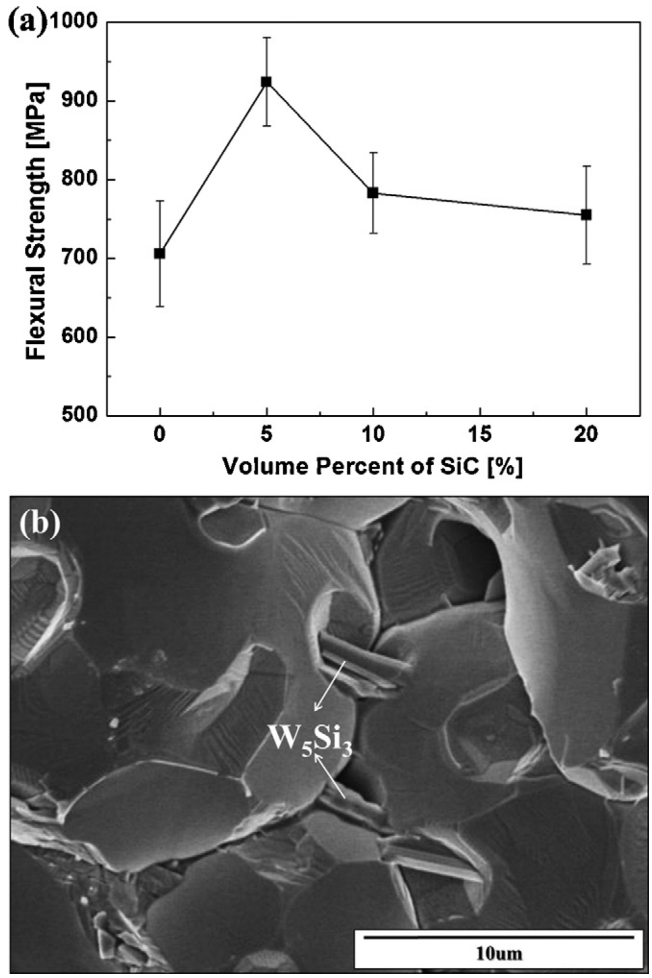

Fig. 3. (a) Variation of the flexural strength of SiC_{NW}/W composites while varying the SiC volume fraction. (b) Fracture surface of the SiC_{NW}/W composites.

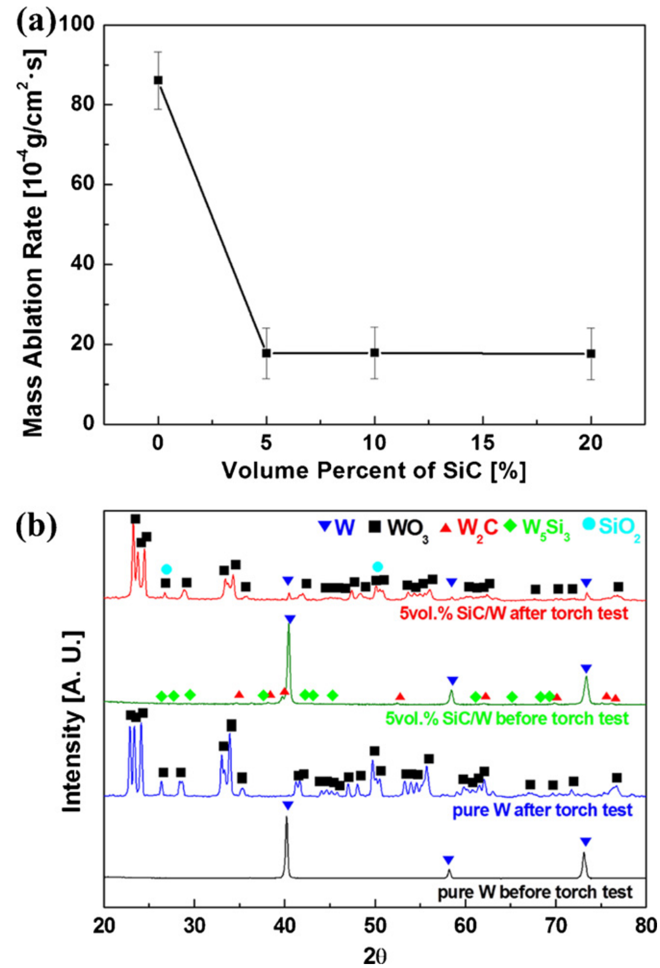

Fig. 4. (a) Mass ablation rate after the oxy-acetylene torch test of the SiC_{NW}/W composites. (b) XRD patterns of specimen surfaces before and after the oxy-acetylene torch test of pure tungsten and the SiC_{NW}/W composites.

5583 device with a crosshead speed of 0.2 mm/min and a span of 4 mm. Flexural strength testing was performed using three-point bending, and the specimen size was 6 mm × 3 mm × 1 mm at room temperature. Ablation tests were carried out with an oxy-acetylene flame. The flow rates of the oxygen and acetylene gas were 12 l/min and 10 l/min, with pressures of 5 bar and 1.5 bar, respectively. A specimen with a diameter of 12 mm was exposed to the flame for a 30 s ablation. The mass ablation ratio was calculated by the weight change before and after the test for each sample.

3. Results and discussion

Fig. 1(a) shows the respective microstructures of the SiC nanowires. SiC nanowires synthesized by a reaction between CNT and SiO powder have diameters of approximately 100–200 nm and lengths similar to those of carbon nanotubes (up to 2–3 μm). The morphology of the SiC nanowire/W (SiC_{NW}/W) composite powders indicated that the SiC nanowires are homogeneously distributed in the W powders, as shown in Fig. 1(b). The particle sizes of the tungsten range from 300 nm to 1 μm. The SiC nanowires maintain their shape and display no chemical reaction during the drying, calcination and hydrogen reduction processes. The key feature of the spray-drying process is that the SiC nanowires are distributed homogeneously in the W powders without any morphology change. Fig. 1(c) and (d) shows the microstructures of the surface of the 5 vol.% SiC_{NW}/W composites and 20 vol.% SiC_{NW}/W composites etched with the Murakami etchant. The composite has three distinct regions. The first region is a round, un-etched area representing W_2C. The second region is an etched area corresponding to the W grain. The third region is an area with rod-type morphology occupied by W_5Si_3. The rod-type W_5Si_3 phase was homogeneously dispersed in the tungsten grain and was randomly oriented. The grain size of each phase is 10–15 μm and the diameter and length of the rod-type W_5Si_3 are approximately 200 nm and 2–3 μm, respectively. The W_2C phases of the 5 vol.% SiC_{NW}/W composites show small grains of about 5–10 μm in size. The grains were located at the boundary among large W grains, as shown in Fig. 1(c); however, the W_2C phases of 20 vol.% SiC_{NW}/W composites show large grains of about 20 μmin size that appear to have coalesced. The relative density of sintered SiC_{NW}/W composites was 95–97%, as measured by the Archimedes method.

X-ray diffraction patterns of the SiC_{NW}/W composites with different volume fractions sintered at 1700 °C for 3 min are shown in Fig. 2(a). Peaks of W, W_2C and W_5Si_3 are identifiable [17]. The W_2C and W_5Si_3 phases are stable carbide and stable silicide respectively [18,19]. As the volume percent of SiC increases, the peak intensity of W decreases and the peak intensity of W_2C and W_5Si_3 increases due to the chemical reaction between W and SiC. The intensity of the diffraction peak of the W_2C andW_5Si_3 increased with an increase in the volume fraction of the SiC, clarifying that a larger amount of SiC leads to a larger amount of the metal W taking part in the chemical reaction and therefore larger amounts of W_2C and W_5Si_3 being produced. According to Seng and Branes [20], the possible reactions between W and SiC can be expressed as follows:

$$SiC + \frac{5}{3}W \rightarrow \frac{1}{3}W_5Si_3 + C \tag{1}$$

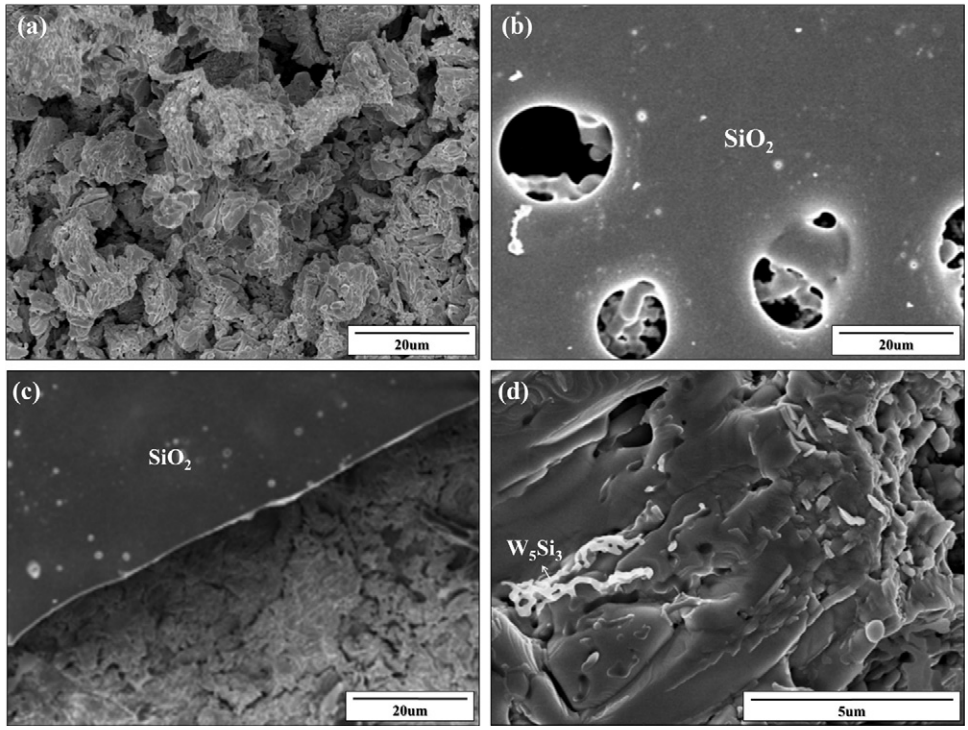

Fig. 5. SEM images of specimen surfaces of pure tungsten (a) and 5 vol.% SiC_{NW}/W composites (b), (c) after the oxy-acetylene torch test. (d) High-magnification SEM image of the specimen surfaces of the 5 vol.% SiC_{NW}/W composites after the oxy-acetylene torch test.

$$SiC + \frac{5}{2}W \rightarrow \frac{1}{2}WSi_2 + W_2C \quad (2)$$

$$SiC + \frac{3}{2}W \rightarrow \frac{1}{2}WSi_2 + WC \quad (3)$$

$$SiC + \frac{8}{3}W \rightarrow \frac{1}{3}W_5Si_3 + WC \quad (4)$$

With an increase in the temperature, the formation of W_5Si_3 and WC directly from the reaction of W with SiC (reaction (4)) is kinetically more favorable, after which WC changes into the stable carbide W_2C.

Fig. 2(b) shows the EDS results of the 20 vol.% SiC_{NW}/W composites. EDS was used to confirm the elemental analysis of the different regions. Peaks corresponding to tungsten alone were obtained in region 1. Peaks related to W and C were obtained in region 2. Region 3 gave peaks that corresponded to W and Si, confirming the existence of W_5Si_3. Fig. 2(c) shows TEM micrographs and selected-area electron diffraction (SAED) patterns of the same composites. Fig. 2(c) shows SAED patterns of the W_2C, W, and W_5Si_3 phases. The W_2C phases have a hexagonal crystal structure, the W phases have a cubic crystal structure, and the W_5Si_3 phases have a tetragonal crystal structure. The volume fractions of the W, W_2C and W_5Si_3 phases as a function of the volume percent of SiC are shown in Fig. 2(d). As shown in Fig. 2(d), the volume fraction of tungsten decreased as the SiC content increased. The volume fraction of the W_5Si_3 and W_2C phases also increased as a function of the SiC content. W_5Si_3 and W_2C phases were the major phases of the composite containing 20 vol.% of SiC nanowires.

Fig. 3(a) shows the flexural strength of the SiC_{NW}/W composite and the monolithic tungsten. The flexural strength reaches its maximal value, 924 MPa, in the 5 vol.% SiC nanowire, after which the values decrease as the SiC content increase. The maximum value of flexural strength at 5 vol.% SiC_{NW}/W results from the dispersion of the rod-type W_5Si_3 phases and the small grain size the W_2C phases in the W matrix. However, when SiC in excess of 5 vol.% was added, the volume fractions of the hard and brittle W_2C phases increased and the grain size and agglomeration of the W_2C drastically increased, as shown in Fig. 1(c) and (d). This effect reduced the flexural strength [21,22]. The fracture surface of the sintered SiC_{NW}/W composites is shown in Fig. 3(b). The rod-type W_5Si_3 phases are shown to be dispersed within the tungsten grains or at the grain boundaries of the tungsten matrix as shown in Fig. 3(b). The fractography of the composite fabricated with SiC nanowire followed reactive sintering shows clear evidence of the pulled-out W_5Si_3 and the bridging effect of W_5Si_3, which indicates that the rod-type W_5Si_3 bears significant stress by sharing a portion of the load. Therefore, it is expected that the rod-type W_5Si_3 dispersed in the tungsten matrix simultaneously strengthen the composite [23].

The high-temperature ablation property of SiC_{NW}/W composites was investigated, as shown in Fig. 4(a). The mass ablation rate of the SiC_{NW}/W composites was 18×10^{-4} g/cm^2 s, while that of pure tungsten was around 86×10^{-4} g/cm^2 s. It is well known that the deterioration of the ablation resistance in pure tungsten is due to the formation of porous tungsten oxide, which is easily swept away during ablation testing. The XRD results shown in Fig. 4(b) show that the pure tungsten was completely oxidized after the torch test, whereas W peaks remained in the SiC_{NW}/W composites after the torch test. Hence, these W peaks of the SiC_{NW}/W composites, which survived after the torch test, are good evidence that the addition of SiC assists SiC_{NW}/W composites in enduring elevated temperatures. As shown in Fig. 5(b)–(d), a thin SiO_2 layer formed by the oxidation of W_5Si_3 developed at the surface of the SiC_{NW}/W composites after the torch test. Moreover, the unoxidized rod-type W_5Si_3 phases prevent the removal of tungsten oxide. Therefore, the SiC_{NW}/W composites appear to have a low ablation rate due to the thin SiO_2 layer that formed on the surface of the specimens after the torch test and due to the presence of the rod-type W_5Si_3 phases, whereas the pure tungsten showed serious ablation and a porous surface after the torch test, as shown in Fig. 5(a).

4. Conclusions

In summary, SiC_{NW}/W composites were fabricated by a spray-drying process followed by reactive sintering in an effort to investigate the effect of their addition on the microstructure and mechanical properties of tungsten composites augmented with SiC nanowire. W_2C and W_5Si_3 phases were formed by a reaction between the SiC and the W during the sintering process. Due to the bridging phenomenon by rod-type W_5Si_3 phase, the flexural strength at room temperature was significantly increased from 706 MPa to 924 MPa. In oxy-acetylene torch testing, the mass ablation rate was improved by approximately four times in the SiC_{NW}/W composites compared to that of pure tungsten. Therefore, tungsten composites augmented with SiC nanowire are promising candidates for high-temperature applications.

Acknowledgements

This research was supported by NSL (National Space Lab) program through the Korea Science and Engineering Foundation funded by the Ministry of Education, Science and Technology (N01110292).

References

[1] J.S. Moya, S. Lopez-Esteban, C. Pecharroman, Prog. Mater. Sci. 52 (2007) 1017–1090.
[2] H.-K. Kang, Scr. Mater. 51 (2004) 1051–1055.
[3] T. Zhang, Y. Wang, Y. Zhou, G. Song, Int. J. Refract. Met. Hard Mater. 28 (2010) 498–502.
[4] H. Kishimoto, T. Shibayama, K. Shimoda, T. Kobayashi, A. Kohyama, J. Nucl. Mater., in press, doi:10.1016/j.jnucmat.2010.12.079.
[5] A. Mattern, B. Huchler, D. Staudenecker, R. Oberacker, A. Nagel, M.J. Hoffmann, J. Eur. Ceram. Soc. 24 (2004) 3399–3408.
[6] S.W.H. Yih, C.T. Wang, Tungsten—Sources, Metallurgy, Properties and Application, Plenum Press, New York, 1979, p. 151.
[7] J. Roger, F. Audubert, Y. Le Petitcorps, J. Mater. Sci. 43 (2008) 3938–3945.
[8] K.E. Rea, V. Viswanathan, A. Kruize, J.Th.M. De Hosson, S. O'Dell, T. McKechnie, S. Rajagopalan, R. Vaidyanathan, S. Seal, Mater. Sci. Eng. A 477 (2008) 350–357.
[9] M. Roosta, H. Baharvandi, Int. J. Refract. Met. Hard Mater. 28 (2010) 587–592.
[10] M.A. Yar, S. Wahlberg, H. Bergqvist, H.G. Salem, M. Johnsson, M. Muhammed, J. Nucl. Mater. 408 (2) (2011) 129–135.
[11] G. Matsuo, T. Shibayama, H. Kishimoto, K. Hamada, S. Watanabe, J. Nucl. Mater., in press, doi:10.1016/j.jnucmat.2011.02.005.
[12] L. Baud, C. Jaussaud, R. Madar, C. Bernard, J.S. Chen, M.A. Nicolet, Mater. Sci. Eng. B 29 (1995) 126–130.
[13] R.-j. Zhang, Y.-q. Yang, W.-t. Shen, C. Wang, Thin Solid Films 519 (2010) 1367–1370.
[14] Z. Pan, H.-L. Lai, F.C.K. Au, X. Duan, W. Zhou, W. Shi, N. Wang, C.-S. Lee, N.-B. Wong, S.-T. Lee, S. Xie, Adv. Mater. 12 (16) (2000) 1186–1190.
[15] Y. Morisada, M. Maeda, T. Shibayanagi, Y. Miyamoto, J. Am. Ceram. Soc. 87 (5) (2004) 804–808.
[16] M. Omori, Mater. Sci. Eng. A 287 (2000) 183–188.
[17] Joint Committee for Powder Diffraction Studies (JCPDS): W (PDF #89-3012), W_2C (PDF #79-0743), W_5Si_3 (PDF #51-0941).
[18] S. Coskun, M.L. Ovecoglu, B. Ozkal, M. Tanoglu, J. Alloys Compd. 492 (2010) 576–584.
[19] S.J. Son, K.H. Park, Y. Katoh, A. Kohyama, J. Nucl. Mater. 329–333 (2004) 1549–1552.
[20] W.F. Seng, P.A. Barnes, Mater. Sci. Eng. B 72 (2000) 13–18.
[21] S. Tzamtzis, N.S. Barekar, N. Hari Babu, J. Patel, B.K. Dhindaw, Z. Fan, Composites Part A 40 (2009) 144–151.
[22] G.-M. Song, Y.-J. Wang, Y. Zhou, Int. J. Refract. Met. Hard Mater. 21 (2003) 1–12.
[23] G. Garces, G. Bruno, A. Wanner, Acta Mater. 55 (2007) 5389–5400.